

## Superconducting Cavity Quenching in the Presence of Magnetic Field

T. Khabiboulline, J. Ozelis, D. Sergatskov, I. Terechkin

### I. Introduction

Level of magnetic field on walls of superconducting RF structures affects their performance; so if a focusing lens or a corrector in a cryomodule is in the vicinity of an accelerating resonator, extent of possible quality factor degradation must be carefully analyzed. Especially it is true for accelerating systems where cavities with high quality factors are used, like in high power linear superconducting RF linacs working in the CW mode of operation. The issue was investigated by many authors (see references [1] to [5]), and is considered well understood. Based on this understanding, practical requirements for allowed magnetic field on walls of cavities were established that range from 1  $\mu$ T in the case of TESLA-type 1.3 GHz cryomodule [6, p. 281] to 10  $\mu$ T in the case of the HINS linac 325 MHz system [7]. It worth to mention though that all the studies in the referenced sources were using RF cavities immersed in the magnetic field applied before the walls of the cavities became superconducting.

On the other hand, it is known that many superconducting RF structures work successfully in the vicinity of magnetic devices and do not experience significant drop in the quality factor (e.g. see [8] and [9]); this happens because the magnetic field, if not too strong, cannot penetrate superconducting walls of cavities that were cooled down before the field was applied. In [9] an attempt was made to observe a superconducting spoke resonator's quality factor degradation induced by magnetic field of coils installed in the vicinity of the cavity and activated after the cavity became superconducting; no degradation was observed until a superconducting coil was used to generate stronger magnetic field, and until it was placed closer to the quench spot, which was on the surface of one of the spokes and thus was shielded from the coil's field by the outer wall of the cavity.

In the situation typical for RF cavities of a linac, flux lines generated by a magnetic device penetrate wall of a cavity only when the cavity quenches and a "warm hole" makes it possible for the magnetic field to enter the cavity. Flux lines associated with this field must also exit the cavity through the same hole. Because part of the flux can be trapped in the wall, degradation of the quality factor can occur; the amount of the trapped flux will define a degree of this degradation. Known correspondence between the amount of the trapped flux and the associated quality factor degradation can allow less conservative evaluation of acceptable magnetic field on walls of superconducting cavities, which can result in simpler designs of magnetic elements in accelerating cryomodules.

The normal conducting zone in a superconducting wall of a cavity that develops during quenching allows some magnetic flux inside the cavity; this flux is partially trapped after the stored energy is dissipated and the walls turn cold again. Due to the appearance of normal-conducting spots in cavity walls associated with the trapped flux, surface temperature in the vicinity of the initial quench spot increases, and subsequent quenches are anchored to the same area. If these quenches happen in the "no magnetic field" environment (e.g. when the power

supplies of the magnets are off), corresponding part of the wall heats above the transition temperature, trapped flux annihilates, and the initial quality factor of the cavity restores (at least partially). We will call this process quench annealing.

To understand this process quantitatively, tests using two 1.3 GHz elliptical one-cell cavities were made in June and then in August of 2011, and subsequent modeling of the flux trapping process was attempted to better understand the data obtained during the tests. The comparison of the test data with the modeling results helps to validate the developed modeling technique before applying it towards a search for justified requirements for allowed fringe magnetic field of beam optics elements installed inside a cryomodule.

## II. Test setup and test data collection

To generate relatively strong magnetic field on walls of tested cavities, a superconducting test coil was fabricated using NbTi strand. List of the coil parameters is shown below:

- Inner diameter of the winding	70 mm
- Outer diameter of the winding	90 mm
- Length of the winding	46.2 mm
- Number of turns	4046
- NbTi strand diameter (52-filament, 1.3 Cu/nCu ratio)	0.5 mm
- Expected quench current @ 4.2 K	144 A
- Transfer function for the center of the coil	416.7 G/A
- Transfer function on the axis at 60 mm from the center	161.8 G/A

Cavities were tested using the FNAL's Vertical Cavity Test Facility (VCTF) [10]. Because only standard feed-through connectors are available at this facility, the maximum current of 20 A could only be used. Nevertheless, the magnetic field on the walls of the cavity could easily exceed the critical field ( $B_{c2} \approx 0.2$  T) of pure (RRR 300) Nb used for cavity fabrication.

Two 1.3 GHz, one-cell cavities with known position of a quench spot were used in the tests: TE1ACC-002 in the first test (it will be called **Cavity#1** in this note) and TE1ACC-001 (**Cavity#2**) in the second one. In both cases, the test coil was installed near wall of a tested cavity, in the vicinity of a known quench spot, which, in both studied cases, was in the equator area, but located at different angles relative to the position of the test coil (Fig. 1). In both tests, the position angle was estimated earlier by thermal measurements using Cernox temperature sensors located along the equator of the cavity [11]. The angles were found to be  $\sim 30^\circ \pm 5^\circ$  for the Cavity#1 and  $\sim 45^\circ \pm 5^\circ$  for the Cavity#2.

The test procedure was similar for both cavities. First, current into the test coil was increased to a desired level. Second, the level of the accelerating gradient in the tested cavity was gradually increased until the first quench was observed. The magnetic field trapped during this quench resulted in the increase of local surface resistance and in some drop of the quality factor immediately after the quench. Levels of the accelerating gradients before and after the first quench were recorded. Next, with continuing quenching, the test coil current was set to zero and the level of the accelerating gradient was gradually increased to keep the cavity quenching. After

a stable quenching gradient was reached, this new value of the accelerating gradient and corresponding quality factor were recorded.

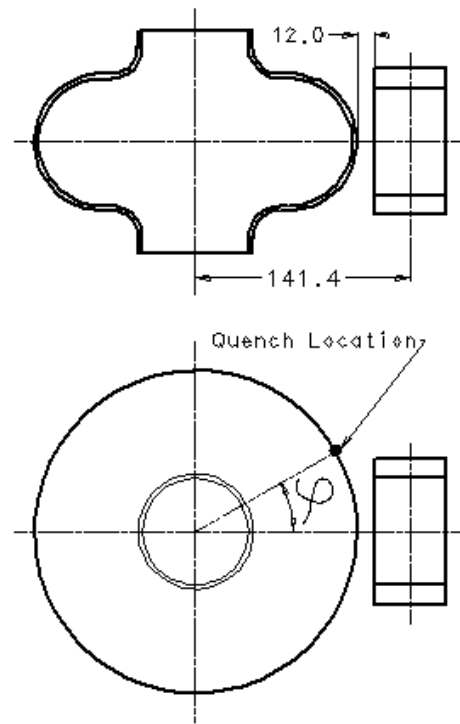


Fig. 1: Relative position of the test coil, and the quench spot location on the surface of a 1.3 GHz elliptical cavity.

### Testing Cavity#1

The initial (with zero magnetic field) quality factor of the cavity was  $2.71 \cdot 10^{10}$  at the accelerating gradient of  $\sim 25.4$  MV/m; the accelerating gradient at quench was  $\sim 33.3$  MV/m.

Table 1 below shows data obtained during the test. In this table,  $I$  is the excitation current of the test coil (in mA),  $E_{aq}$  and  $Q_{aq}$  are the accelerating gradient (in MV/m) and the quality factor recorded **after** the first **quench** with the external magnetic field,  $E_{an}$  and  $Q_{an}$  are the accelerating gradient and the quality factor after “annealing” (that is repetitive quenching with “zero” external magnetic field resulting in the heating of the affected area and annihilation of the trapped fluxions).

Fig. 2 illustrated the data in the Table 1 showing the quality factor as a function of the coil current for two states: the quality factor after quenching in the presence of the current in the coil (blue curve for  $Q_{aq}$ ), and the quality factor after quenching with the current in the coil is set to zero (the red curve for  $Q_{an}$ ). The figure also demonstrates irreversible degradation of the quality factor if the current in the test coil is higher than 10 mA. If the current was below 10 mA, it was possible to fully restore the “before quench” quality factor. The bump in the end of the current

scale in Fig. 2 is, most probably, of artificial nature, that is due to some defects in the measurements or interpretation (see additional notes below, in the test #2 chapter).

Table 1. Data obtained during test with the coil #1

I [mA]	$Q_{aq}$	$Q_{an}$	$E_{aq}$ [MV/m]	$E_{an}$ [MV/m]
0.1	2.79E+10		33.7	
1	2.71E+10	2.76E+10	33.3	33.7
2	1.88E+10	2.64E+10	33.4	33.6
5	1.26E+10	2.77E+10	33.1	33.6
10	8.33E+09	2.77E+10	32.9	33.6
20	4.69E+09	1.29E+10	28.2	32.5
30	4.33E+09	1.25E+10	25.4	32.8
50	2.71E+09	1.24E+10	22.3	32.9
70	2.5E+09	1.17E+10	20.5	32.3
100	2.4E+09	1.28E+10	18.5	32.5
150	4.9E+09	1.25E+10	16.2	32.5
200	3E+09	1.25E+10	14.2	32.8
300	1.5E+09		11.5	

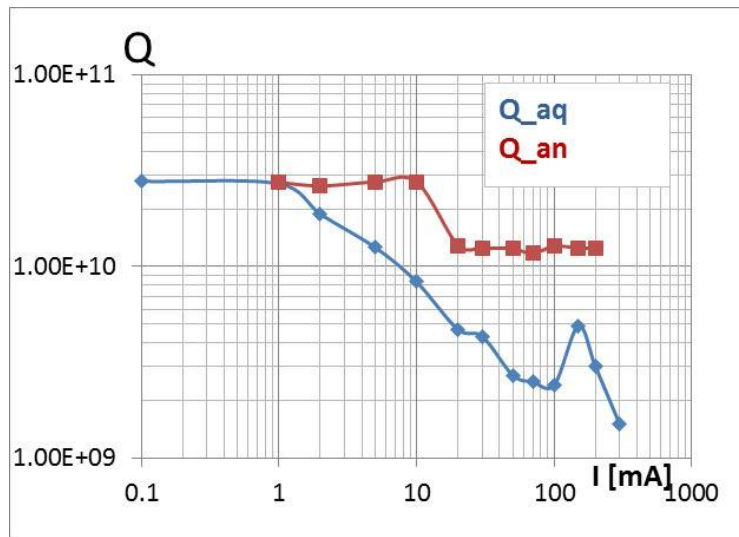


Fig. 2. Quality factor of the cavity after quenching with (blue curve) and without (red curve) magnetic field generated by the coil.

Graph in Fig. 3 shows how the accelerating gradient drops after the quench with the magnetic field on and to which extent it is restored by the RF quench annealing. For all current levels used in the test, it was possible to restore the “before quench” level of the accelerating gradient by increasing the input power.

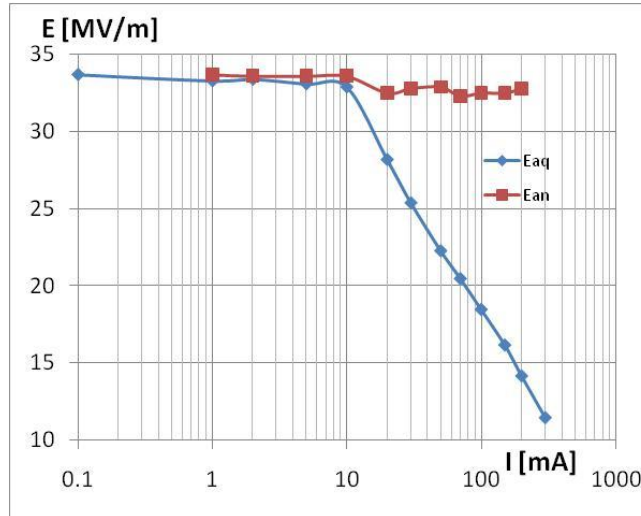


Fig. 3. Maximum accelerating gradient as a function of the coil current after quench with the magnetic field on (red curve) and after quench annealing (blue curve).

Testing Cavity#2

During this test, besides the quality factor **Q** at the maximum level of the accelerating gradient, the quality factor at 10 MV/m (**Q10**) was used as a reliable reference point; the initial value of this quantity for the Cavity#2 was measured to be  $Q_{10} = 2.52 \cdot 10^{10}$ . Before any magnetic field was applied, the maximum accelerating gradient of ~31.1 MV/m was achieved. Table 3 summarizes the test; here **Q10<sub>aq</sub>** and **Q10<sub>an</sub>** refer to quality factor measured at 10 MV/m after the first **quench** with the magnetic field and after “**annealing**” with no magnetic field. Figures 4 to 6 visualize the data in the Table 3.

Table 3. Data obtained during test with the coil #2

I (mA)	E <sub>aq</sub> [MV/m]	E <sub>an</sub> [MV/m]	$10^{-10} \cdot Q_{10_{aq}}$	$10^{-10} \cdot Q_{10_{an}}$	$10^{-10} \cdot Q_{aq}$	$10^{-10} \cdot Q_{an}$
0	31.1		2.52	2.52	1.82	1.82
1	31.1		2.12	2.52	1.67	1.81
1.78	31.16	31.22	2.11	2.36	1.55	1.82
3.16	30.92	31.15	1.9	2.31	1.37	1.81
5.62	31.04	31.24	1.61	2.31	1.1	1.83
10	31.1	31.26	1.28	2.36	0.815	1.84
17.8	31.36		0.635	1.64		1.2
-1.78		30.96	1.67	1.73	1.2	1.2
-3.16	31.2	30.95	1.57	1.78	1.05	1.2
31.6	22.42	31.47	0.335	2.24	0.22	1.7
56.2	19.35	31.42	0.173	2.24	0.123	1.84
100		31.14	0.097	1.36		1.12
31.6		31.4		2.26		1.78

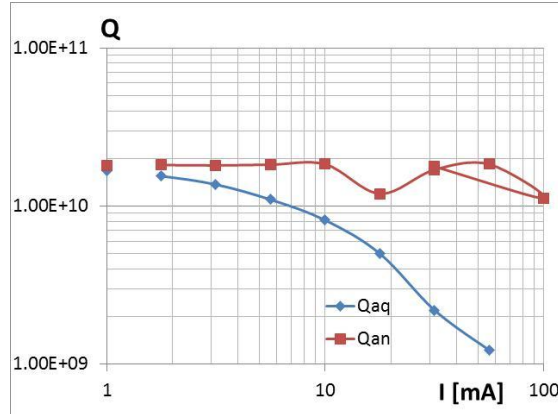


Fig. 4. Quality factor of the cavity after quenching with and without magnetic field generated by the coil. Measured at the maximum field level.

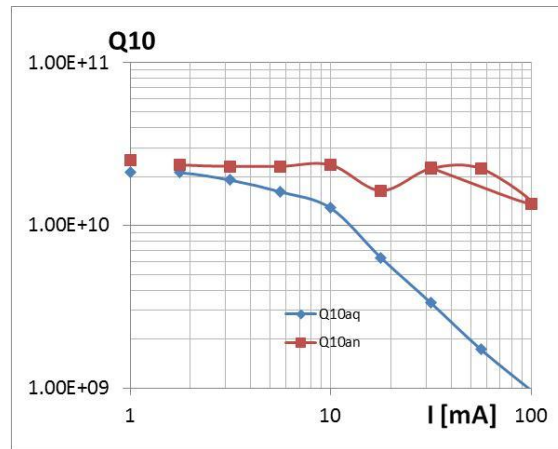


Fig. 5. Quality factor of the cavity after quenching with and without magnetic field generated by the coil. Measured at 10 MV/m electric field

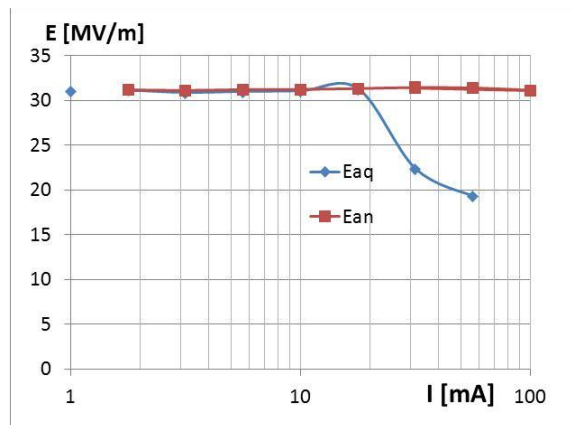


Fig. 6. Maximum accelerating gradient after quench in magnetic field and after quench annealing as a function of the coil current.

Curves in the figures above are qualitatively quite similar to those obtained during the first test. Comparing corresponding graphs, we can observe the following:

1. In both cases, the drop in the quality factor becomes noticeable starting with the current  $I \approx 1$  mA. The quality factor drops  $\sim 15$  times when the excitation current reaches  $\sim 100$  mA.
2. There is no “mystery” glitch found in the second set of measurements, so the most probable reason for the glitch in Fig. 2 was a typo.
3. In the second test, it appeared possible to restore the quality factor to its initial level with the current in the test coil up to  $\sim 60$  mA. The drop in the corresponding curve in the first test at  $\sim 10$  mA (Fig. 3 ) was, probably, a result of overlook because the annealing effect, although anticipated to some extent, was not an expected result at **these high** current levels, and was not actively looked for.
4. The accelerating gradient (and the quality factor) could be fully restored in the second test in the total current range after a possibility of the “annealing” was discovered at  $\sim 30$  mA (see figures 4 to 6). The fact that the annealing process resulted in much better restoration for the Cavity#2 is attributed to better persistence (and more test time available) towards finding a way to restore the cavity performance without warming up the cavity.

### III. Evaluating degradation of the quality factor

Knowing geometry, winding parameters of the test coil, and its position in the test setup relative to the quench spot, it is possible to evaluate by modeling the drop of the cavity quality factor. Main uncertainties in this modeling are position of the initial quench spot and the size of a “warm hole” that develops in the superconducting surface of the cavity during quenching. Values of these parameters are not so easy to obtain; nevertheless, careful **thermal measurements** can provide some information about both of them, and **quench propagation modeling** can be used to narrow the range for the “warm hole” size. The modeling precision, in turn, depends on the knowledge of material properties at cryogenic temperatures and the heat transfer factor from the surface of cavity into liquid Helium; values of these parameters are also known with relatively high uncertainty. In spite of all these uncertainties, it appeared possible to obtain results that have some sense.

We will assume that the “warm hole” is centered on the equator of the cavity and will make a parametric sweep using the diameter of the hole and the position angle  $\varphi$  (Fig. 1) as parameters. Fig. 7 demonstrates magnetic field distribution on the walls of a one-cell, 1.3 GHz, elliptical superconducting cavity. The magnetic field generated by the coil does not penetrate inside the cavity; on the s/c surface it reaches 300 G at 1 A coil current. The field in the quench area depends on the position angle  $\varphi$ ; e.g. at  $\varphi = 30^\circ$ , the field within the area where the warm hole appears after quench reaches 150 G. When the cavity is warm, the field freely penetrates inside (Fig. 8). Maximum field on the surface in this case is 120 Gs at 1 A. With a “warm hole” on the superconducting surface, part of the flux penetrates inside the cavity (Fig. 9).

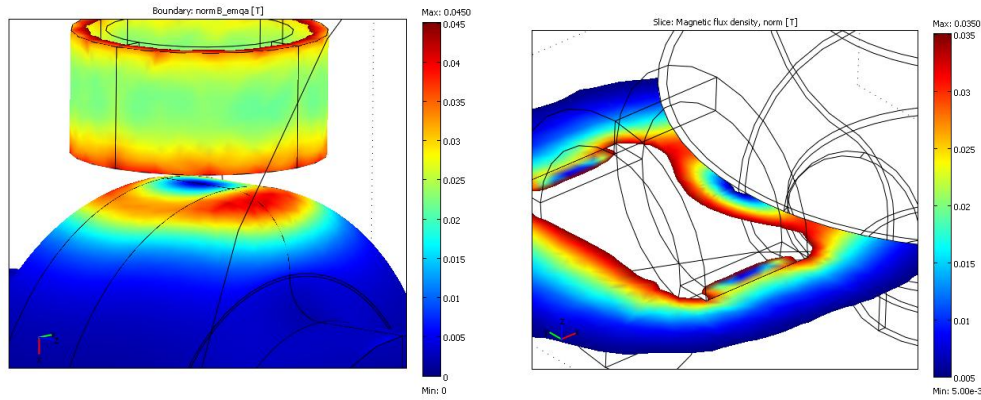


Fig. 7. Field map for the test coil near the one-cell 1.3 GHz elliptical superconducting cavity. No field penetrates through the cavity wall.

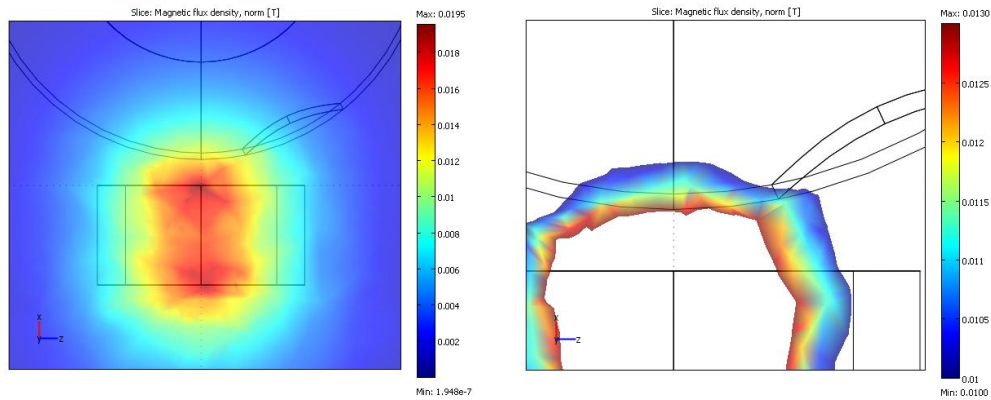


Fig. 8. The test coil near a normal conducting cavity. Cavity walls do not matter.

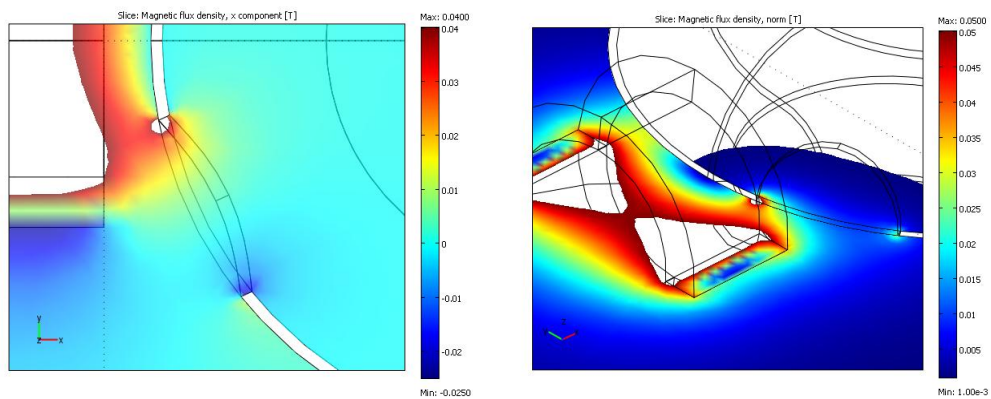


Fig. 9. Warm hole ( $D = 50$  mm,  $\phi = 30^\circ$ ) in the wall of a 1-cell 1.3 GHz superconducting cavity. The magnetic field penetrates through the warm opening.

Knowing distribution of the magnetic field in the presence of a “warm hole”, we can evaluate the magnetic flux penetrating inside the cavity through the hole; this flux must leave the cavity through the same hole. The penetrating flux can be found by integrating the next vector expression, which calculates only the flux that enters into the cavity:

$$\mathbf{F}_{\text{in}} = (\mathbf{n} \cdot \mathbf{B}) \cdot (\mathbf{n} \cdot \mathbf{B} > 0)$$

Similar vector expression can be written that calculates the flux that is coming out:

$$\mathbf{F}_{\text{out}} = (\mathbf{n} \cdot \mathbf{B}) \cdot (\mathbf{n} \cdot \mathbf{B} < 0)$$

Logical expressions  $\mathbf{n} \cdot \mathbf{B} > 0$  or  $\mathbf{n} \cdot \mathbf{B} < 0$  control the direction of the flux in the expressions. Fig. 10 illustrates the case in Fig. 9 by showing the flux through the warm hole; the three windows represent three components of the flux:  $F_x$ ,  $F_y$ , and  $F_z$ , with the axis X directed along the axis of the test coil.

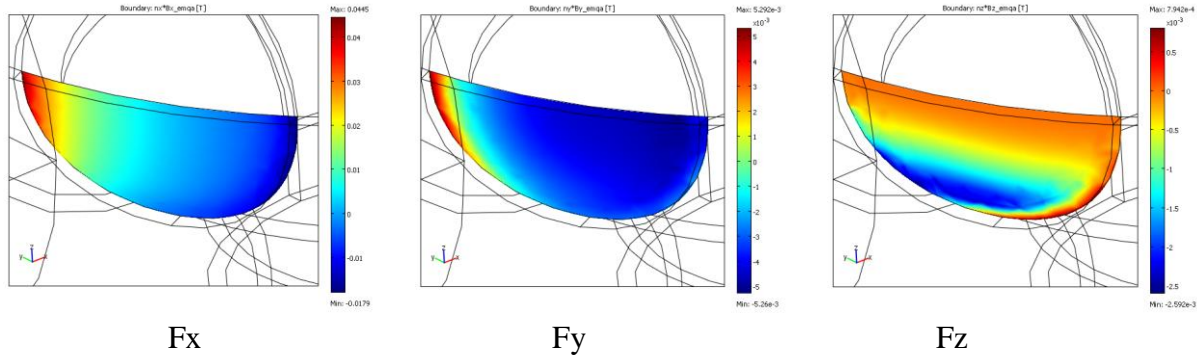


Fig. 10 Magnetic flux components within the warm hole

Knowing the flux penetrating the cavity wall, it is possible to evaluate expected degradation of the quality factor and compare it with the measured one. Let's assume that all the flux lines stay trapped by the Nb wall after the "warm" hole turns "cold" and all the surface of the cavity returns to the superconducting state (this assumption is supported by series of tests made in Sacleby by C. Vallet in 1990 [5]). The flux quantum value is

$$\mathbf{F}_0 = \mathbf{h}/2\mathbf{e} = 2 \cdot 10^{-15} \text{ T} \cdot \mathbf{m}^2.$$

We need to take into account the flux that crosses the "warm" surface inside the cavity in both directions; we will call it "crossing" flux. So, we expect totally

$$N = (\mathbf{F}_{\text{in}} - \mathbf{F}_{\text{out}}) / \mathbf{F}_0$$

normal conducting spots with the flux penetrations through the surface, where  $\mathbf{F}_{\text{in}}$  and  $\mathbf{F}_{\text{out}}$  are the fluxes entering and exiting the "warm hole" (with corresponding signs). The effective radius of each normal-conducting core associated with one flux quant is defined by the coherence length (see p. 71 and p. 174 in [6]):

$$\xi_0 = (\mathbf{h} \cdot \mathbf{v}_F) / (\mathbf{k}_B \cdot \mathbf{T}_c).$$

The normal-conducting surface area due to the "crossing" flux is then

$$S_n = \pi \cdot \xi_0^2 \cdot N.$$

Within this surface area, Nb is at 2K, but is not superconducting, so the surface resistance of Nb can be found based on the skin layer approach:

$$R_s = 1 / (\sigma_{2K} \cdot \delta) = \text{sqrt}(\pi \cdot \mathbf{f} \cdot \mu_0 / \sigma_{2K}).$$

For Nb with RRR=300,  $\sigma_{2K} = 2.2 \cdot 10^9 \text{ (Ohm} \cdot \mathbf{m})^{-1}$  (see Fig. 3.2 in [6], p. 59), and at 1.3 GHz, we expect  $R_s \approx 1.5 \cdot 10^{-3} \text{ Ohm}$ .

Now power loss in the wall can be evaluated:

$$P_n = \frac{1}{2} \cdot \mathbf{J}_s^2 \cdot \mathbf{R}_s \cdot \mathbf{S}_n = \frac{1}{2} \cdot \mathbf{H}_t^2 \cdot \mathbf{R}_s \cdot \mathbf{S}_n,$$

where  $\mathbf{J}_s$  is the amplitude of the surface current density in the cavity at the location of quench, which is equal to the amplitude of the tangential magnetic field  $\mathbf{H}_t$  in the same area.

Knowing the power loss, we can calculate expected quality factor after quenching in the magnetic field. By definition, the quality factor

$$Q = \omega \cdot W / P_{\text{loss}}.$$

The energy  $W$  stored in the cavity is proportional to  $\mathbf{H}_t^2$ :

$$W = k_H \cdot \mathbf{H}_t^2,$$

so we can write down:

$$Q = \omega \cdot k_H \cdot \mathbf{H}_t^2 / (P_0 + P_n),$$

where  $P_0$  is the power loss in the cavity without the trapped flux. Then expression for the total quality factor can be written as

$$1/Q = 1/Q_0 + (\mathbf{R}_s \cdot \mathbf{S}_n) / (2 \cdot \omega \cdot k_H),$$

And we can talk about the “field-induced” part of the quality factor  $Q_{\text{FI}}$ :

$$Q_{\text{FI}} = 2 \cdot \omega \cdot k_H / (\mathbf{R}_s \cdot \mathbf{S}_n)$$

Coefficient  $k_H$  for the 1.3 GHz elliptical cavity referring to the RF magnetic field on the equator was evaluated by RF modeling [12]:

$$k_H = 1.3 \cdot 10^{-9} \text{ J/(A/m)}^2$$

Having in mind that, for Nb,  $\xi_0 = 39 \cdot 10^{-9} \text{ m}$  (i.g. see [6], p. 71), and that we know the initial quality factors  $Q_0$  of the tested cavities, we have all needed information to evaluate the drop in the quality factor.

Required magnetic modeling was made using COMSOL 4.2 AC module with the “warm” hole diameter  $D$  and the azimuthal position of the initial quench spot  $\varphi$  used as parameters. Corresponding data, that cover both tests, are shown in Table 4, where **the total “crossing” flux** is shown for a 1 A current in the coil. The range of parameters in the table was chosen based of the results of measurements and the initially assumed position of the initial quench spot and the “warm hole” diameter.

Table 4. Total “crossing” flux (in  $\mu\text{Wb}$ ) through the “warm” hole at 1 A of the test coil current

$\varphi \setminus D$	40 mm	50 mm	60 mm	70 mm
0°	6.43	14.03	25.22	39.53
10°	12.85	21.63	32.48	44.95
20°	14.68	23.17	32.97	43.79
25°	11.96	19.38	28.20	38.18
30°	8.49	14.30	21.64	30.39
35°	5.58	9.66	15.13	22.11
40°	3.60	6.30	10.04	15.06
45°	2.35	4.12	6.61	9.98
50°	1.56	2.74	4.39	6.65

The data in the table is illustrated by plots in Fig. 11 and Fig. 12. A contour plot in Fig. 11 shows “crossing” (trapped) flux levels (in  $\mu Wb$ ) on the plane ( $\varphi, D$ ).

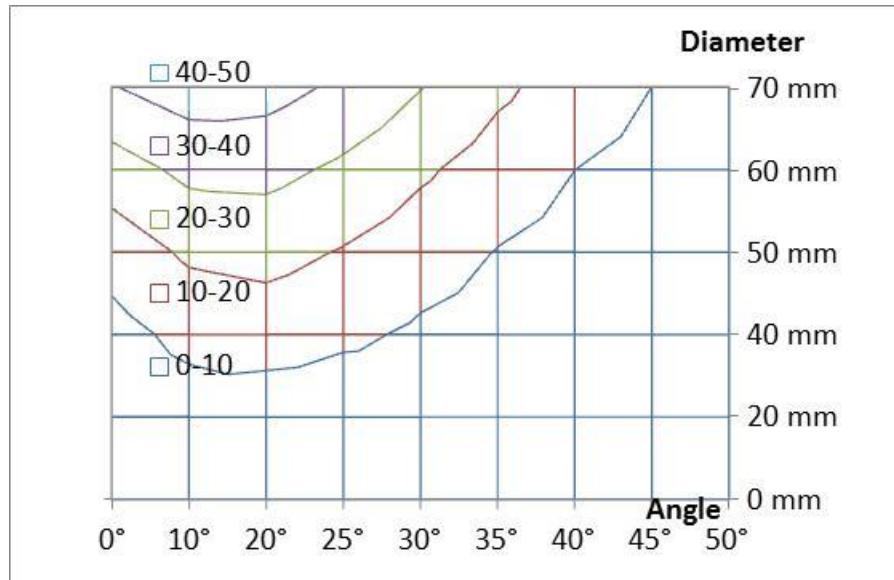


Fig. 11. “Crossing” flux contour plot at  $I = 1$  A; values in the legend are in  $\mu Wb$ .

Fig. 12 shows how the flux at 1 A of the coil current depends on the angle for several values of the hole diameter, and also the dependence of the flux on the diameter of the warm hole for several values of the position angle. The dependence on the diameter is close to quadratic for combination of angles and diameters when the hole stays clear of the coil-cavity symmetry plane ( $\varphi \geq 20^\circ$  in our case); it is close to cubic for the case  $\varphi = 0^\circ$ .

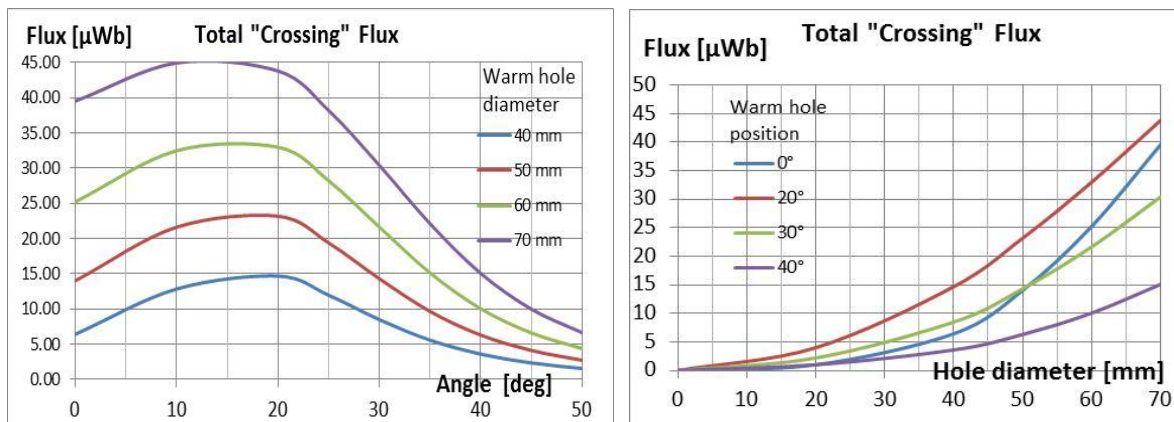


Fig. 12. Dependence of the flux crossing the cavity surface in both directions on the angular position of the warm hole and on the hole diameter

From Fig. 11 follows that the same “crossing” flux (and hence corresponding quality factor) can be obtained along a certain line on the plane ( $\varphi, D$ ). For example, a  $10 \mu Wb$  flux (at 1 A current in the test coil) is observed when ( $\varphi, D$ ) combinations are ( $5^\circ, 40$  mm), ( $15^\circ, 30$  mm),

(28°, 40 mm), (35°, 50 mm), (40°, 60 mm), or (45°, 70 mm). To know what exactly combination of parameters we are dealing with in each test, some additional information is needed about the position angle and the maximum diameter of the warm hole. This information can be provided either by direct measurements, or by modeling. Because of the uncertainty in the choice of right combination of the parameters, figures below compare the measured “after quench” quality factor with the modeling prediction for several ( $\phi$ ,  $D$ ) combinations.

In Fig. 13, a fit is made to the data obtained during the test using the **Cavity#1** (see Table 1 and associated figures). The warm hole diameter of 70 mm and the initial quench position at ~20° provides a good fit to the measurement data. Analyzing level lines in Fig. 11, one can see that position angles of more than ~20° (initial guess, based on the thermal measurements, was ~30°) can be combined only with larger diameter of the warm hole:  $D > 70$  mm.

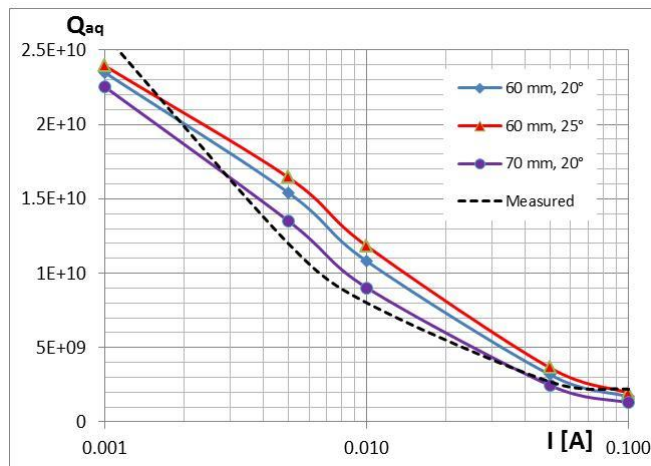


Fig. 13. Measured and estimated quality factor for the Cavity#1

In Fig. 14, a fit is made to the data obtained during the test using the **Cavity#2** (see Table 2 and associated figures).

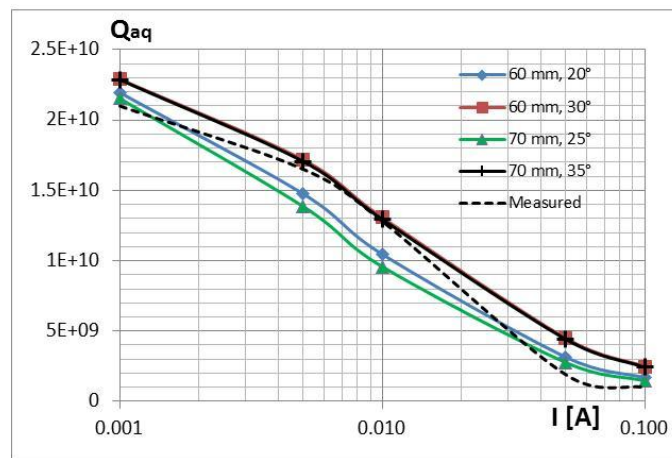


Fig. 14. Measured and estimated quality factor for the Cavity#2.

Analysis of Fig. 14 suggests that to make a fit to the measurement data, we can use a combination of the initial quench position angle of more than  $\sim 35^\circ$  (the initial guess based on the measurement was  $\sim 45^\circ$ ) and the hole diameter of more than  $\sim 70$  mm. Although combinations with smaller diameters and position angles can also explain the measurement results, the quench position angle found in [11], can only be combined with the hole of 70 mm or more in diameter. So, both tests point towards “warm hole” diameter of more than  $\sim 70$  mm.

As was mentioned, to choose the right set of parameters, additional information is needed about the initial point of quench or/and about the size of the “warm hole”. It is difficult to predict where quench is going to happen, so a method (or combination of methods) to obtain this information must be found, like thermometry, second sound, optical means, or other. It is also possible to try to fix the quench spot using an external spot heater.

Modeling can also be applied to narrow the range of possible parameters. For example, in [13] and [14], an attempt was made to model quench propagation in walls of superconducting RF cavities that can provide information about diameter of the “warm hole”.

#### IV. Modeling development of a “warm hole”

Cavity quality factor during quench event is defined by the normal conducting surface area in the “warm hole” and by the surface temperature. For a one-cell, 1.3 GHz elliptical superconducting cavity with the area of a “warm” surface of  $\sim 1000$  mm<sup>2</sup>, we can expect the quality factor  $Q \approx 10^6$ . This defines the time constant of the energy decay process:  $\tau \approx 1$  ms. The energy stored in the cavity with the gradient of  $\sim 30$  MV/m just before quenching is  $\sim 14$  J, so the energy dissipation rate  $P \approx 14$  kW. On the other hand, we can assume the cavity wall cooling rate by liquid Helium of  $\sim 1$  W/cm<sup>2</sup>, which results in  $\sim 10$  W of the total cooling power. This means that the initial stage of quench propagation can be studied in the adiabatic approximation. To obtain information about the size of the “warm hole”, and to observe collapse of the warm hole, cooling by liquid Helium must be taken into account during modeling.

In [13], the adiabatic approximation is used to solve the heat balance equation:

$$C(T) \cdot \partial T / \partial t = \text{div}(K(T) \cdot \text{grad}(T)) + \frac{1}{2} |H_t|^2 \cdot R_s(T),$$

where  $C(T)$  and  $K(T)$  is specific heat and thermal conductivity of Nb,  $H_t$  is the RF magnetic field on the surface, and  $R_s$  is the surface resistance. Fig. 15 show accepted in [13] dependence of these quantities on the temperature.

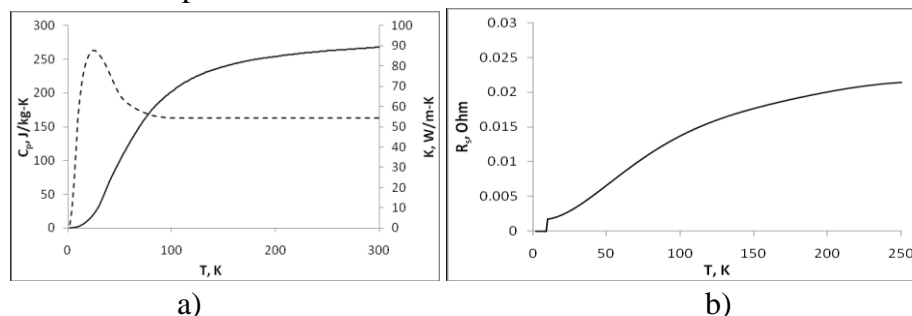


Fig. 15. Specific heat (a, solid curve), thermal conductivity (a, dashed curve), and surface resistance at 1.3 GHz (b) of Nb as functions of temperature.

The heat balance equation is combined with the RF energy dissipation equation

$$\partial W/\partial t = -1/2 \cdot |H_t|^2 \cdot \int R_s(T) \cdot dA,$$

where the integral is taken across the normal conduction area of the cavity surface:  $T > T_c$ .

The problem was solved using MATLAB programming environment. Fig. 16 shows how the size (diameter) of the warm hole changes with time during quenching for different assumed initial energy, which depends on the type of a cavity (one-cell or nine-cell) and the accelerating gradient at quench.

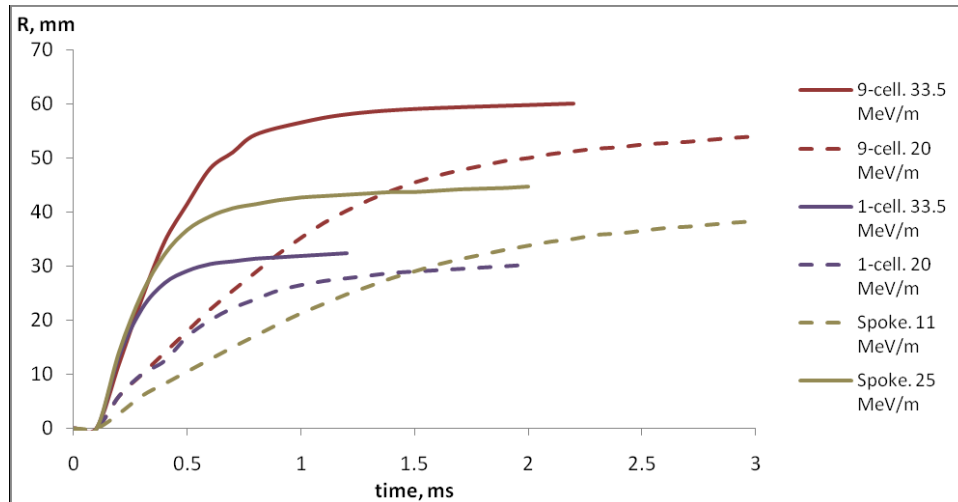


Fig. 16. Normal zone radius as a function of time for different types of cavities and initial RF energy

Obviously, we cannot find the warm hole diameter in the adiabatic case; nevertheless, the data in Fig. 16 indicate that for 1-cell cavity with the initial gradient of 33.5 MV/m, the warm hole radius can easily become larger than 30 mm.

In [14], quench propagation problem was studied using transient heat propagation module of the COMSOL Multi-Physics modeling suite. The system of equations was quite similar to what was used in [13]. A simple 2D axially symmetric geometry was used where the top surface of a 3-mm thick disk made of Nb was heated by RF current during quenching event and the bottom surface was insulated or cooled by liquid Helium. Three cases were studied: adiabatic case, cooling by liquid Helium at 4.2 K, and cooling by LHe at 2 K (He-II). Development of quench is very similar in all the three cases. The time scale of the energy dissipation in the conducting layer is  $\sim 0.5$  ms, which is consistent with the findings in [13]. Redistribution of the deposited heat takes much longer time. If **He-I** is used for cooling, the maximum diameter of 78 mm is reached in  $\sim 100$  ms; if **He-II** is used, a  $\sim 73$ -mm hole is observed in  $\sim 70$  ms. The “warm hole” disappears at  $\sim 200$  ms in the first case and in  $\sim 190$  ms in the second one. It takes much longer for the whole sample to come to the initial (and uniform) temperature state.

Fig. 17 shows how the temperature distribution along the bottom surface of the sample cooled by He-II changes with time. At  $t < 1$  ms, the temperature front propagates radially and the average temperature gradually increases as the heat reaches through the thickness of the sample.

At the moment  $t \approx 25$  ms, the maximum average temperature is observed, and the cooling process starts to prevail; the maximum temperature on the bottom surface is  $\sim 44$  K at this moment. At  $\sim 190$  ms, the maximum temperature of the surface becomes below the transition temperature for Nb: 9.2 K.

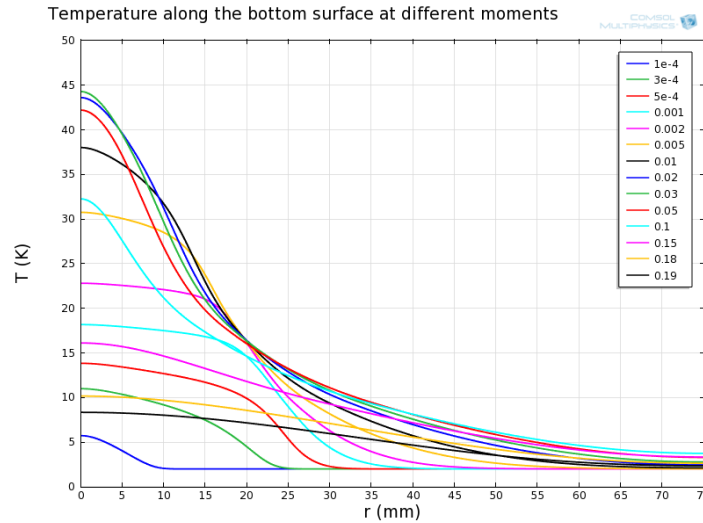


Fig. 17. Temperature distribution on the cooled surface at different moments after quench; the values in the legend are in seconds.

Quench propagation rate in the initial stage of the process derived from the data obtained in [14] is quantitatively similar to what can be derived from Fig. 16 for the case of one-cell cavity at 33.5 MV/m [13] and is  $\sim 125$  m/s, and it takes only  $\sim 0.3$  ms to form a 25 mm diameter hole in the superconducting wall.

It was stressed in [14] that the heat transfer coefficient to LHe-II is not well known for the test environment close to what we had during the tests, and fitting expressions used to model the "warm hole" development for the case of the cooling by He-II are not so precise. Analysis of data in references [7] and [8] in [14] tells that there are two major temperature regions related to the heat transfer in LHe-II: a small (less than  $\sim 2$  K) and a large temperature difference (more than  $\sim 10$  K) between cooled surface and liquid Helium bath. For the first region, the data for the Kapitza conductance can be expressed by a simple formula:

$$h_K = \alpha \cdot T^n$$

with  $n \approx 3$  and  $\alpha \approx 430$  W/(m<sup>2</sup>·K). For the second region, where the energy flux density exceeds  $\sim 10^4$  W/m<sup>2</sup>, and where our data show we are, the data strongly depends on geometry and on the size of samples; there is no readily available data that would correspond to the case of the cavity we used during the test. Nevertheless, parametric expression used in [14] for He-II environment results in a warm hole diameter of  $\sim 73$  mm that is in agreement with the predictions of the quality factor degradation modeling (more than 70 mm) which are based on the measurement results shown in Fig. 11 and Fig. 12.

## Conclusion

An attempt to understand dynamics of quench propagation in walls of a superconducting cavity was made by using a sample coil that creates magnetic field outside the cavity and is mounted in the vicinity of the quench spot. Temperature of Nb surface was measured using Cernox sensors; the cavity quality factor before and after quench was recorded at different current settings in the test coil. The recorded quality factors were compared with predictions of a computational model that allowed to narrow the range for the diameter of the “warm hole” in the cavity wall after quench. The modeling in [14] shows that the hole diameter reaches ~72.5 mm if 2K He is used for cooling, which agrees with the evaluation made using the observed quality factor degradation due to penetration of magnetic field into a cavity though a warm hole developed in the cavity wall after quenching.

An important observation was made during the measurements: the initial quality factor (before quench) can be restored if subsequent quenches are made in the absence of the magnetic field. This finding, if analyzed and used properly, can allow significant relaxation of the fringe field requirement for a focusing lens installed near superconducting cavity in a cryomodule of an RF linac.

## References:

- [1] P. Kneisel and B. Lewis, “Additional RF Surface Resistance in Superconducting Nb Cavities Caused by Trapped Magnetic Flux”, Jeff. Lab, Tech. Note #94-028.
- [2] Kenji Saito, “RRR Effect on the Flux Trapping of Niobium SC Cavities”, SRF-2003.
- [3] J. Knobloch, H. Padamsee, “Flux Trapping in Niobium Cavities During Breakdown Events”, Workshop on RF Superconductivity, Padova, Italy, 1997; proceedings, pp. 337 – 343.
- [4] M. Ono, et al, “Magnetic Field Effects on Superconducting Cavities”, SRF-1999.
- [5] C. Vallet, et al, “Flux Trapping in Superconducting Cavities”, EPAC-1992, p. 1295.
- [6] H. Padamsee, et al, RF Superconductivity for Accelerators, Wiley Press, 1998.
- [7] T. Khabiboulline, I. Terechkine, “HINS Front End Superconducting Cavity Magnetic Field Requirements”, FNAL note TD-08-006, 2008.
- [8] R.A. Laxdal, et al, “Cryogenic, Magnetic, and RF Performance of the ISAC-II Medium Beta Cryomodule at TRIUMF”, PAC 2005, Knoxville, TN, USA, Proceedings, p. 3191.
- [9] R. Madrak, et al, “First High Power Pulsed Tests of a Dressed 325 MHz Superconducting Single Spoke Resonator at Fermilab”, PAC 2011, TUP076.
- [10] J. P. Ozelis, et al, “Design and Commissioning of Fermilab’s Vertical Test Stand for ILC SRF Cavities”, PAC-07, Proceedings, p. 2283.
- [11] D. Sergatskov, private communication.
- [12] T. Khabiboulline, private communication.
- [13] S. Antipov, et. al, “2-D simulation of Quench Dynamics”, FNAL note, TD-11-017.
- [14] I. Terechkine, “Modeling Quench Propagation in Superconducting Cavity Using COMSOL”, FNAL note TD-11-019, Nov. 2011.